VARIABILITY OF PLANETARY MASS COMPANION 2M1207 B

Yifan Zhou, Daniel Apai, Glenn Schneider, ...
The University of Arizona
Draft version August 27, 2015

ABSTRACT

Rotational modulations in disk-integrated light of brown dwarfs have recently provided powerful constraints on the properties of ultracool atmospheres, including longitudinal and vertical cloud structures and cloud evolution. Furthermore, detection of periodic light curve variations can directly probe the rotational periods of ultracool objects.

We present here, for the first time, time-resolved high-precision photometric measurements of a planetary-mass companion, 2MASS1207b, to a brown dwarf primary. Using HST/WFC3 and point spread function combination with two spacecraft roll angles we detect photometric modulations in the light curve. The amplitude is 0.9% in the F160W and 1.5% in the F125W filters; we find a consistent period and similar phase in both bands. Joint fit to the lightcurve in both bands suggest a period of $10.2^{+0.9}_{-0.8}$ h. The relative amplitudes in the two filters are very similar to that found in a recent study of a field (high-gravity) L-dwarf, suggesting that the cloud structures that introduce the photometric modulations are similar in high- and low-gravity objects. Importantly, our study also measures, for the first time, the rotational period for directly imaged planetary-mass companion.

Subject headings: brown dwarfs – planets and satellites: atmospheres – planets and satellites: individual (2M1207b) – techniques: photometric

1. INTRODUCTION

Cloud properties in high- and low-gravity objects – thick clouds: an explanation for very red and faint near-infrared fluxes of directly imaged planets

Rotational mapping is powerful: successes in brown dwarfs...

The target 2M1207b... contrast The key challenge of obtaining the lightcurve of 2M1207b is the high contrast to and small separation from 2M1207A.

In this Letter we present the first high-contrast, high-precision, time-resolved observations of a directly imaged planet or planetary-mass object. We successfully detect rotational modulation and measure the amplitudes in two bands and determine the rotational period.

2. OBSERVATION

We obtained direct images of the 2M1207A+b system on UT 2014 April 11from 08:07:47 to 16:53:18 using the Hubble Space Telescope (HST) and its Wide Field Camera 3 (WFC3, Kimble et al. 2008) in the frame of the HST Proposal GO-13418 (PI: D. Apai). We acquired the observations in filters F125W ($\lambda_{\rm pivot}$ = 1245.9 nm, full width at half maximum (FWHM) = 301.5 nm) and F160W ($\lambda_{\rm pivot}$ 1540.52, FWHM = 287.9 nm), roughly corresponding to the J and H bands. The WFC3 pixel scale is ≈13mas. We used the 256×256 pixels sub-array mode to avoid memory dumps during the observations. In order to provide a near-continuous coverage for detecting modulations we observed the 2M1207 system in six consecutive HST orbits, obtaining data with cadence of ~ 1.5 minutes over a baseline of 8 hours and 40 minutes. The observations were interrupted by 58 minute-long Earth occultations every 94 minutes.

The observations applied space craft rolls between each two orbits to allow roll-subtraction of the primary (e.g. Song et al. 2006). The telescope roll angles for orbits 1,

3, and 5, and those taken in orbits 2, 4, and 6 differed by $25°$. At the separation of 2M1207b this angle difference corresponds to a displacement of $0.34''$ or 2.75 and 2.30 resolution elements in F125W and F160W, respectively. In each orbit we took thirteen SPARS10 non-destructive read-outs with NSAMP=10, alternating between F160W and F125W filters, with 2–3 identical exposures in one exposure sequence. To improve PSF sampling and reduce the risk caused by bad pixels, we applied standard 4 point dithering. Over the 6 orbits, we obtained 70 images with 10 non-destructive read-outs in F125W and 64 images in F160W with exposure time of 88.4 s in each filters.

3. DATA REDUCTION

3.1. *Photometry*

We started the reduction from the the `flt` files files produced by the WFC3's `calwfc3` pipeline. We did not opt to use the more advance `ima` files pipeline products because these provided less information on 2M1207A, which saturated after the first few read-outs. The `flt` files are results of basic calibration, including dark current correction, non-linearity correction, flat field correction, as well as up-the-ramp fit on the non-destructive read-outs also considering cosmic rays. From the beginning, pixels with data quality flags "bad detector pixels" (DQ = 4), "unstable response" (DQ = 32), and "bad or uncertain flat value" (DQ = 512) were masked out and excluded from further analysis as suggested by previous transit exoplanet spectroscopic observations(e.g. Berta et al. 2012; Kreidberg et al. 2014).

One major challenge of high contrast imaging observation using WFC3/IR is significant under-sampling of the detector. 2M1207 A and b are only separated by ~ 6 pixels or ~ 5 FWHM of the PSF. When applying roll subtraction, notable artifact structures are generated by image interpolation and shifting. On the other hand,
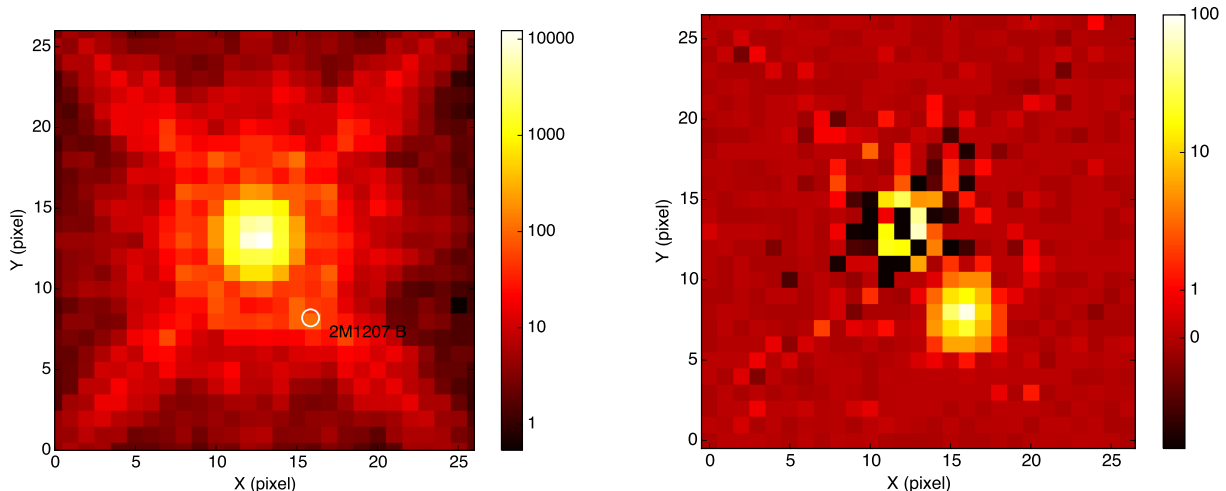
FIG. 1.— WFC3 F160W images of 2M1207A system. *Upper panel*: In the original image 2M1207 B is hidden in the halo of the bright 2M1207A. *Lower panel:* In the residual image – after the subtraction of the hybrid PSF – 2M1207 B is detected at a high significant level.

Tiny Tim PSF simulator([Krist 1995](#)) offers a solution by providing Nyquist sampled PSF, but significant systematic errors of *Tiny Tim* PSF limits its ability in high precision photometry([Biretta 2014](#)). However, 6 orbits of observation provides us a chance to fully characterize the difference of model and observed PSFs. To obtain robust *Tiny Tim* PSF photometry, we designed a 2-round PSF fitting strategy: 1. calculating correction map for *Tiny Tim*; 2. hybrid PSF photometry.

For both of 2 rounds, we used *Tiny Tim* to calculate $10\times$ over-sampled model PSFs based the filters, the spectra ([Bonnefoy et al. 2014](#); [Patience et al. 2010](#)), the telescope's actual focus, and the telescope jitter. We used the new set of Tiny Tim parameters provided by [Biretta](#) ([2014](#)) to better model the cold mask, diffraction spikes, and the coma. The focus parameters were calculated using the model listed on the STScI website[1]. We determined the exact position of 2M1207A first by fitting the PSF on a dynamic coordinate grid and minimizing the difference in the observed and modeled PSFs at a region centered on 2M1207 A with a 5-pixel-radius aperture centered 2M1207 b excluded.Then we fit the position of 2M1207 b and the photometries of 2M1207 A and b together by least square optimization. From our data set, we discovered that the difference of observed PSFs and model PSFs are very stable for given PSF position. Therefore at the end of the first round PSF fitting, we derived 8 (2 roll angles $\times$ 4 dithering positions) empirical correction maps for each filter:

$$\mathrm{Corr} = \mathrm{Median}(\mathrm{PSF_{model}} - \mathrm{PSF_{obs}}) \qquad (1)$$

where $\mathrm{PSF_{model}}$ is a combination of two *Tiny Tim* PSFs for 2M1207 A and b. In the second round, we combined the correction term linearly with the two *Tiny Tim* PSFs to generate hybrid PSFs, and fitted for their amplitudes together. We found that by including the correction term, the reduced χ^2 of PSF fitting is decreased from ~ 10 to around unity. Because the total fluxes of the model PSFs were normalized to unity as default, the fluxes of 2M1207 A and B were solely represented by the amplitude of the two PSFs coordinately.

[1] http://www.stsci.edu/hst/observatory/focus/FocusModel

However, PSF profiles change with different exposure positions due to pixelation, especially for the case that WFC3 IR is significantly under-sampled. Also, the flat fields may potentially have large scale structures ([Dressel 2012](#)). Because of these factors, the fluxes for both 2M1207 A and B are correlated with the dithering position. To break the correlation, we normalize each group of exposures that have the same dithering position and roll angle individually – we took the median of the fluxes that were measured from these exposures as normalization factors and devided them from every photometric measurement. Because the normalization factor for each group of exposures is calculated across the whole observation, this normalization step have negligible impacts on variability analysis.

3.2. *Uncertainty Analysis: White noise*

We consider the primary source of uncertainty for every measurement is photon noise. We propagated the photon noises of every single pixel that were calculated from count rates and detector gain, to the PSF fitting results. The photon noises for photometry in F125W and F160W are 1.33% and 1.02%, respectively.

Since the primary and secondary PSFs were fitted simultaneously in our PSF photometry procedure, the uncertainties of photometry and position for the primary and secondary are coupled with each other. The second order uncertainty could also contribute to the overall uncertainty, e.g. the imperfection of position measurement of 2M1207A can affect the photometry of 2M1207b. We used a Monte Carlo (MC) method to evaluate the complete systematic of the PSF fitting. We applied the PSF photometry to images that were added with random Poisson noise and repeat the procedure for 1000 time. From the distribution of the result, the uncertainty for F125W and F160W photometry are found to be 1.34% and 1.12%, respectively. We conclude that the white noise of our observation is dominated by photon noise.

3.3. *Uncertainty Analysis: Flat field uncertainties*

In our observations 2M1207 B were observed at 8 different spots on the detector (2 rolls × 4 dithering positions). Imperfect flat field correction are potential sources of
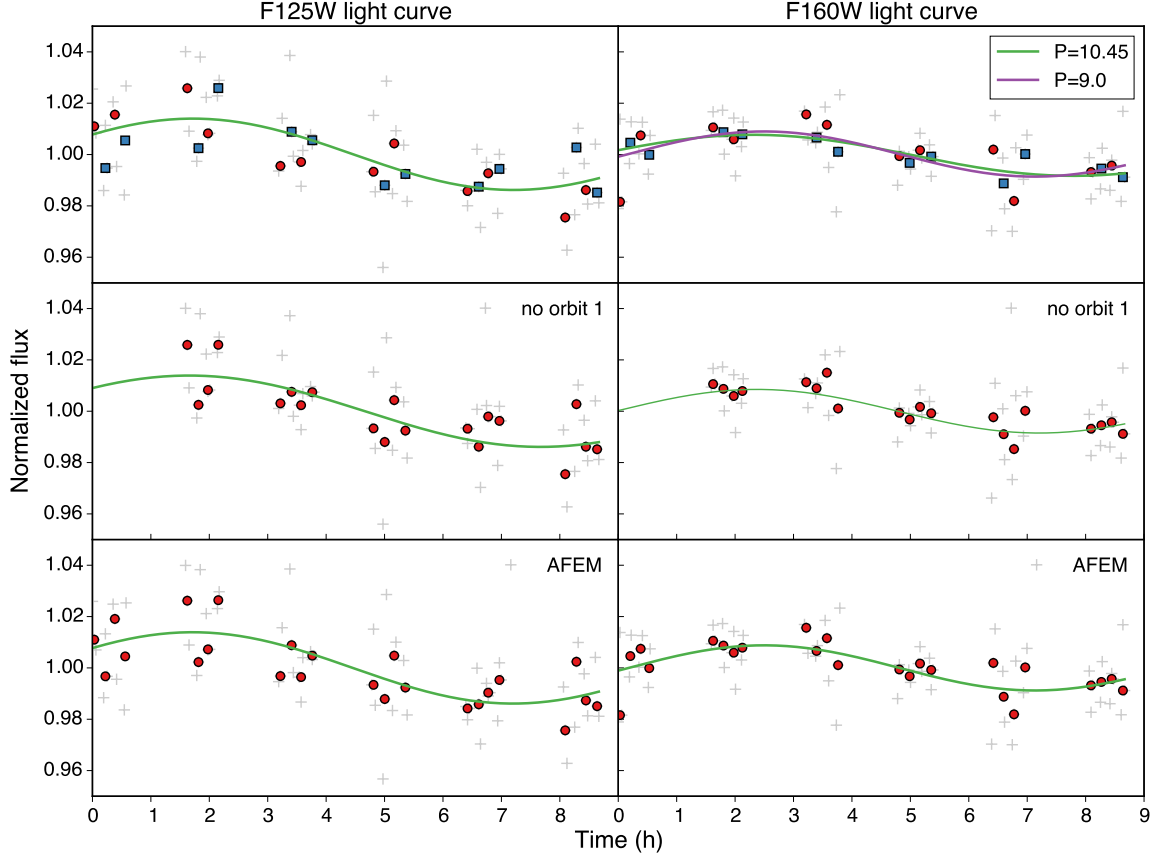
FIG. 2.— F125W (left) and F160W (right) light curves under different verification tests. Individual measurements are plotted with gray crosses. Photometries of the same exposure sequence are binned, and binned data are plotted with points and squares. Fitted sinusoidal waves are plotted with solid lines. *Upper*: binned photometries taken in dithering position 1 and 3 (red points) and that taken in 2 and 4 (blue squares) are plotted differently. They demonstrate same trend of variation. In upper left panel, sinusoidal wave fitted with all parameter set free, and that fitted with period set the same as that of F125W are plotted with green and purple lines, respectively. *Middle*: sinusoidal waves fitted without using the data taken in Orbit 1 are plotted. These curves are almost identical to the curves plotted in upper panel. *Lower*: photometry measured with AFEM-applied images and their best fitted sinusoidal curves are plotted. These photometries and curves are also almost identical to those plotted in upper panel.

variation as they may introduce position-dependent differences in the count rates. The uncertainty of WFC3 IR pipeline flat field is $\sim 1\%$ (Dressel 2012). In PSF photometry, however, multiple pixels are fitted simultaneously and we expect a lower than 1% uncertainty from the flat field errors. To verify this we multiplied every image by an artificial flat field error mask (AFEM) – a uniformly distributed Gaussian noise array with mean of 1 and sigma of 1% – and repeated the PSF photometry on the resulting images. The analysis of these experiments showed almost identical lightcurve to the original, verifying that the flat field errors do not affect our photometry significantly (Figure 2).

4. VERIFICATION OF PHOTOMETRIC VARIATIONS AND AMPLITUDE ESTIMATE

4.1. *Tests and Verification*

The light curves that resulted from our photometry show apparently sinusoidal modulations, discussed in more details in §5. To verify that these modulations are intrinsic to the object and not result of our data reduction procedure or due to instrumental changes, we carried out three different tests.

First, we fitted sine waves independently to the two fil-

ters to verify the similarity of the signal in the two bands (Figure 2). Inconsistent periods or light curve shapes would argue against a genuine signal. We found that the periods of the best fit sine waves are similar, $10.5^{+1.2}_{-1.3}$h for F125W and $9.1^{+1.1}_{-1.0}$h for F160W. These periods are roughly consistent within the uncertainty. Furthermore, these periods are not close to any timescales over which HST or WFC3 are known to changes.

As a second test we repeated the analysis neglecting the first orbit. The motivation behind this test was that, due to spacecraft thermal settling, the first orbit of HST observations is often slightly unstable and is often neglected in high-precision studies (**citation?**). Indeed, in our analysis 2M1207 A is significantly fainter in the first orbit (Figure 3) than in the subsequent ones. Our analysis based on orbits 2–6 only found essentially identical results to our analysis of orbits 1–6, based on which we conclude that the first less reliable orbit does not affect our results significantly (Figure 2, middle panel).

As a third test we explored whether a subset of images, perhaps imperfectly normalized or correlated with specific instrument states, could be driving the light curves into an apparently sinusoidal shape. To test this possibility we split the data into two temporally overlap-

ping halves: sub-dataset one from dithering positions 1 and 3, and sub-dataset two from dithering positions 2 and 4. For both datasets we repeated our analysis independently. For both of F125W and F160W, two halves demonstrated similar trend of variability as shown in Figure 2. Our analysis detected sinusoidal modulations in *both* sub-datasets and in *both* filters, with periods and amplitudes consistent with those derived from the complete data set (2, upper panel).

These tests demonstrate that the modulation seen in our data are consistently present in the different filters, in the different time segments of the data, and in data obtained in different dithering positions.

4.2. *Amplitude and Period Measurements*

To constrain the uncertainties of the least square optimization results, we used a Monte Carlo(MC) method to improve the fitting. We generated a series of random Gaussian noises with the standard deviation same as the photon noise, added them to the original light curves, and applied least square fit to the new light curves. We repeated above routine for 10000 times and obtained the distribution of the fitting parameters. The distributions for the periods and the amplitudes for F125W and F160W light curves are shown in Figure 4.

5. RESULT

We present the first high-contrast, high-resolution, high-cadence, and high-precision photometry of a directly imaged planet or planetary-mass companion. Our observations reveal a modulation in the light curve of the 5–7 M_J companion 2M1207b, the first detection of modulations in directly imaged ultracool objects. The best fit periods for F125W and F160W are 10.4 and 9.0 hour correspondingly. The amplitudes for the normalized light curves are 1.4% and 0.9% for F125W and F160W light curves.

We obtained high signal to noise photometry series for both 2M1207 A and B (Figure 3). On average, the photometric contrast is 6.52 ± 0.01 mag for F125W and 5.77 ± 0.01 mag for F160W. The difference of F125W contrast from that measured in J-band (Mohanty et al. 2007) and F160W contrast from that measured with NICMOS F160W (Song et al. 2006) is due to the different through-

put profiles of the filters.

In the following we will discuss the amplitude and period of 2M1207B and place this object in the broader context of ultracool atmospheres.

The distributions for the periods demonstrate long tail shaped towards long period, with core region roughly Gaussian. With probability range of 64%(1-σ Gaussian), we estimated the 1-σ range for the periods of F125W and F160W to be $10.5^{+1.3}_{-1.2}$ and $9.1^{+1.1}_{-1.0}$ h, respectively. The period for best fitted sine wave of F125W light curve is longer than that of F160W for 1.5 h that is slight larger 1-σ standard deviation. We also performed a joint MC fit with the two light curves with the assumption that the periods of the variation of the two bands are the same. We derived a period of $10.2^{+0.9}_{-0.8}$ h.

The variation amplitudes in the two bands have significant difference. The distributions of the amplitudes are well described by Gaussian profiles. Fitting the histogram to a Gaussian function, we determined that amplitude distribution of F125W peaks at 1.5% with a standard deviation of 0.3%, and that of F160W have mean and standard deviation of 0.9% and 0.2%, respectively. The peaks of the two histograms separated by more than 2-σ. The variation amplitude of F125W light curve is 1.67 times of that of F160W light curve.

6. CONCLUSIONS

- a data-reduction pipeline is developed to obtain high precision photometry measurement from high contrast WFC3 IR data. For a contrast of ~ 7 magnitudes at an angular separation of $\sim 0.7''$, we obtained photometry measurement for 2M1207 B at precision of about 2-3%.

- time variability for 2M1207 B was discovered, the light curve of 2M1207 B for both two colors can be fitted with a T=10.7 hr sinusoidal curve.

- constrain on the amplitude of the amplitude of the variability. Large amplitude can be excluded. Constraints on the inhomogeniety of the cloud coverage can be inferred – small thickness variance...

- ? The atmosphere and cloud structure of 2M1207 B. How does it compare to the brown dwarf.

REFERENCES

Berta, Z. K., Charbonneau, D., Désert, J.-M., et al. 2012, ApJ, 747, 35
Biretta, J. 2014, Space Telescope WFC Instrument Science Report, 1, 10
Bonnefoy, M., Chauvin, G., Lagrange, A.-M., Rojo, P., Allard, F., Pinte, C., Dumas, C., & Homeier, D. 2014, A&A, 562, A127
Dressel, L. 2012, Wide Field Camera 3, HST Instrument Handbook, 1

Kimble, R. A., MacKenty, J. W., O'Connell, R. W., & Townsend, J. A. 2008, in Society of Photo-Optical Instrumentation Engineers (SPIE) Conference Series, Vol. 7010, Society of Photo-Optical Instrumentation Engineers (SPIE) Conference Series, 1
Kreidberg, L., Bean, J. L., Désert, J.-M., et al. 2014, Nature, 505, 69
Krist, J. 1995, in Astronomical Data Analysis Software and Systems IV, Vol. 77, 349
Mohanty, S., Jayawardhana, R., Huelamo, N., & Mamajek, E. 2007, ApJ, 657, 1064
Patience, J., King, R. R., De Rosa, R. J., & Marois, C. 2010, A&A, 517, A76
Song, I., Schneider, G., Zuckerman, B., Farihi, J., Becklin, E. E., Bessell, M. S., Lowrance, P., & Macintosh, B. A. 2006, ApJ, 652, 724
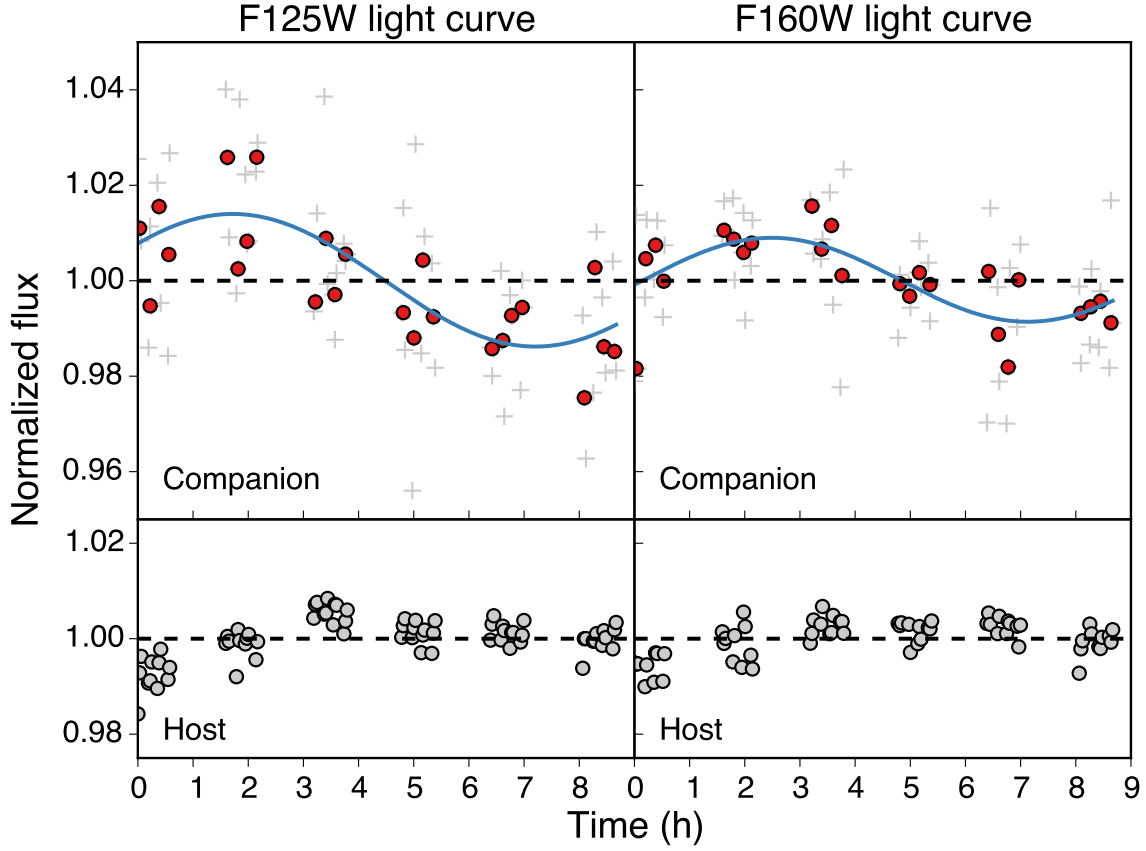
FIG. 3.— Normalized light curves for 2M1207 B (upper) and A (lower) with filter F125W (left) and F160W (right). Individual photometric measurement are plotted in gray crosses and binned photometry are plotted with red points. Best fitted sinusoidal waves are plotted with blue solid lines.
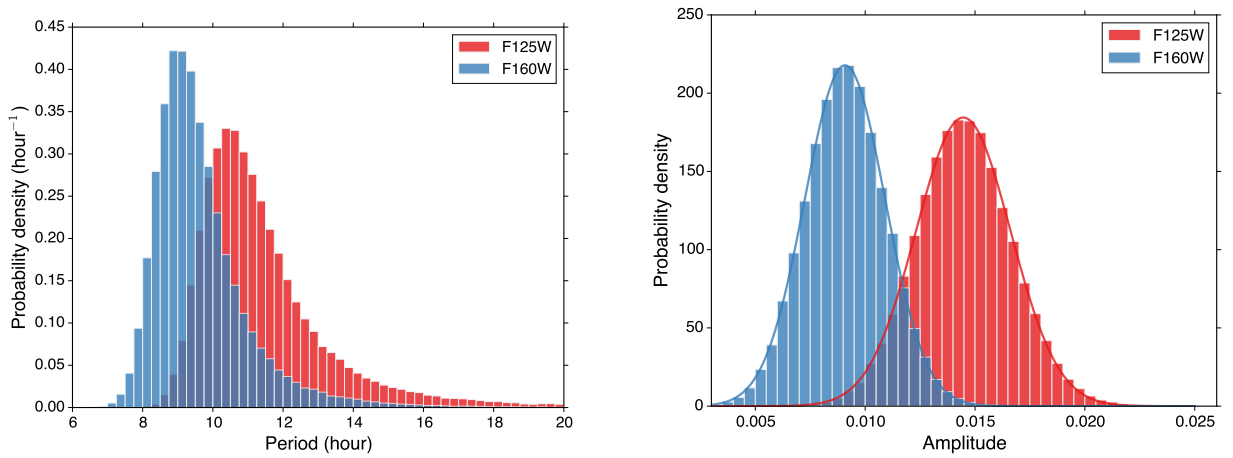

FIG. 4.— Distributions for periods (left) and amplitudes(right) for the light curve of F125W and F160W. The bin size for histograms of period is 0.25 hour and for that of amplitude is 0.5%. Histograms are normalized in the way that total area of the histogram equals to 1. In the right panel, Gaussian profiles are fitted to the histograms and plotted in solid lines.